The Astrophysical Journal, 918:81 (10pp), 2021 September 10 https://doi.org/10.3847/1538-4357/ac0f06

Gas-phase Formation of Cationic Fullerene/Amino Acid Clusters: Evidence for the "Magic Number" Chemical Reactivity of Fullerene Cations

Xiaoyi Hu[1,2,3], Deping Zhang[3,4], Yuanyuan Yang[1,2,3], Yang Chen[3], Liping Qin[1,2], and Junfeng Zhen[1,2,4]
[1] CAS Key Laboratory of Crust-Mantle Materials and Environment, University of Science and Technology of China, Hefei 230026, People's Republic of China; jfzhen@ustc.edu.cn
[2] CAS Center for Excellence in Comparative Planetology, University of Science and Technology of China, Hefei 230026, People's Republic of China
[3] CAS Center for Excellence in Quantum Information and Quantum Physics, Hefei National Laboratory for Physical Sciences at the Microscale, and Department of Chemical Physics, University of Science and Technology of China, Hefei 230026, People's Republic of China
[4] CAS Key Laboratory for Research in Galaxies and Cosmology, Department of Astronomy, University of Science and Technology of China, Hefei 230026, People's Republic of China; lpqin@ustc.edu.cn
Received 2021 April 13; revised 2021 June 14; accepted 2021 June 15; published 2021 September 14

Abstract

An experimental and theoretical investigation on the chemical reactivity of fullerene cations (C_n^+, $n = [36, 60]$) with amino acid molecules (e.g., isoleucine, $C_6H_{13}NO_2$) is performed. The results show that, in the gas phase, fullerene cations can react with amino acid molecules to form fullerene/amino acid cluster cations with high efficiency. The formation rate constants for the ion–molecule collision reactions between fullerene cations and isoleucine are estimated under the pseudo-first-order reaction condition. We find the formation rate constants increase gradually with a declining C-atom number of fullerene cations (C_n^+, $n = [46, 60]$), and depict a plateau in the reactivity for smaller fullerene cations (C_n^+, $n = [36, 44]$). More importantly, by comparing to its neighbor fullerenes, the *magic number* of C-atom counts (54, 58) that process with enhanced chemical reactivity are determined. We also obtained the molecular structures and binding energies for the fullerene-monoisoleucine adducts by quantum chemical calculations, which give a good explanation for the magic number chemical reactivity and the enhanced chemical reactivity of smaller fullerene cations. We infer that our results demonstrate the importance of ion–molecule reactions to the formation of large and complex fullerene-amino acid derivatives in the ISM. The high reactivity of fullerene species may indicate that amino acid molecules or other related prebiotic compounds can accrete on small interstellar carbon dust grains.

Unified Astronomy Thesaurus concepts: Interstellar medium (847); Molecular physics (2058); Interstellar dust processes (838); Polycyclic aromatic hydrocarbons (1280); Astrochemistry (75)

Supporting material: machine-readable table

1. Introduction

Since the discovery of buckminsterfullerene (C_{60}) in the laboratory by Kroto et al. (1985), fullerenes have drawn wide attention, especially on the molecular astrophysics front (Tielens 2013; Bohme 2016, and references therein). Buckminsterfullerene (C_{60}) in space manifested itself through the infrared (IR) spectroscopy of circumstellar and interstellar sources, several near-red diffuse interstellar bands are also linked to the electronic transitions of cationic buckminsterfullerene, C_{60}^+ (see, e.g., Cami et al. 2010; Campbell et al. 2015; Cordiner et al. 2019). In addition, other fullerenes (e.g., in different sizes and structures), and their derivatives (e.g., molecular clusters) may exist in the interstellar medium (ISM) as well (Berné & Tielens 2012; Omont 2016; Cami et al. 2018; Candian et al. 2019).

Experimental and theoretical investigations aimed at revealing the formation mechanism of C_{60} in the interstellar environments have been performed extensively (Zimmerman et al. 1991; Jäger et al. 2011; Berné & Tielens 2012; Zhen et al. 2014). These studies shown that the formation of C_{60} may start from a simple carbon-rich seeded gas, following a bottom-up route (see, e.g., Jäger et al. 2009, 2011), or through UV photodissociation of large polycyclic aromatic hydrocarbon (PAH) molecules, following a top-down route (Berné & Tielens 2012; Zhen et al. 2014). In addition, there is another bottom-up route for the formation of fullerenes from PAHs on grains throughout on-surface synthesis (Otero et al. 2008). These smaller fullerenes may also be involved in both formation routes. Moreover, as a remarkable feature observed in both routes, *magic number* fullerenes with C-atom counts (84, 78, 70, 60, 56, 50, 44, and 36) have been observed (Handschuh et al. 1995). In comparison to their neighbor peaks, the enhanced abundance of these fullerenes implies higher molecular stability (Zimmerman et al. 1991; Zhen et al. 2014; Candian et al. 2019). The stability of fullerenes with C-atom counts ($n = [44, 70]$) was theoretically investigated by Candian et al. (2019) and included the character at three aspects, i.e., the enthalpy of formation per CC bond, the HOMO-LUMO gap, and the energy required to eliminate a C_2 unit. Candian et al. (2019) also suggested that smaller fullerenes with C-atom counts (56, 50, and 44) possibly exist in the astronomical sources.

Fullerenes are known to be electron-deficient polyolefins that can form adducts with many different molecules (Komatsu et al. 1999; Briggs & Miller 2006; García-Hernández & Díaz-Luis 2013a; Garcíia-Hernández et al. 2013b; Sato et al. 2013; Bohme 2016). A critical issue here is to understand the reactivities of the reactions of fullerenes with other molecules (Tielens 2013). Earlier studies by Petrie & Bohme (1993), Bohme (2016), and Zhen et al. (2019a, 2019b) have concluded that fullerenes, e.g., C_{58}^+ and C_{56}^+, have a higher reactivity toward cluster formation than fullerene C_{60}^+.

Recently, our group investigated the formation and photodissociation of fullerene/anthracene, fullerene/9-

vinylanthracene, and fullerene/9-methylanthracene cluster cations (Zhen et al. 2019a, 2019b). The functionalization from aromatic H, methyl, vinyl, to other groups (in here, amino acid group) may change the ease of reaction, the reaction products, or the addition of multiple molecular clusters. We selected amino acids in the present study because of the general astrophysical interest in amino acids (Snyder 1997; Herbst & van Dishoeck 2009; Altwegg et al. 2016). As essential components of proteins and enzymes, they are of fundamental importance and are regarded as a prerequisite for any study on prebiotic compounds that may have been brought to Earth by meteorites (Ehrenfreund & Charnley 2000; Pizzarello et al. 2006). There are two routes that contribute to the gas-phase amino acids that exist in the ISM: one route is, like in the interstellar cloud, a smaller radical will form amino acids or closely related complex organic compounds through gas-phase collision reaction pathways; the other route is the photolysis of plausible presolar ice mixtures on the ice surface, and presolar ice UV photochemistry may be a source of these extraterrestrial amino acids. In the process of warm-up with higher temperatures (or through the photodesorption process), these prebiotic and closely related compounds evaporate from the ice into the gas phase in the molecular cloud (Muñoz Caro et al. 2002; Jäger et al. 2009; Herbst & van Dishoeck 2009).

In this work, we present an investigation of the chemical reactivity of the fullerene cations (C_n^+, $n = [36, 60]$) with amino acid molecules (e.g., isoleucine, Ile, $C_6H_{13}NO_2$, 22 atoms, 131 amu) in the gas phase. Isoleucine is used as the reactant and as examples of interstellar complex organic molecules (e.g., amino acid) based on the following consideration: (1) isoleucine (22 atoms, 131 amu) have a relatively large size in the organic molecules; (2) isoleucine are suitable for heating in the oven that evaporates them into the gas phase efficiently. In the chemical reaction between fullerene cations and amino acid molecules, the amino acid molecule is in excess abundance compared to the fullerene cations, allowing us to roughly estimate the rate constants among different fullerene cations with the pseudo-first-order reaction model. In addition, quantum chemical calculations are performed to determine the molecular structures and the formation mechanisms for the newly formed fullerene/amino acid cluster cations.

2. Experimental Results

The experiments were performed on the apparatus equipped with a quadrupole ion trap and reflection time-of-flight mass spectrometer (experimental details provided in supporting information) (Zhen et al. 2019a, 2019b). C_{60}^+ was generated by the electron impact ionization and filled into the trap within the time range of 0.0−4.0 s, and then a 355 nm laser (~30 mJ/pulse, 10 Hz, irradiation times amounting to 1.8 s, from 4.0 −5.8 s) was used to irradiate the trapped ions to generate smaller fullerene cations. Under laser irradiation, the trapped fullerene cations underwent photofragmentation processes, i.e., they successively lost C_2 units to form a series of smaller fullerene cations (C_n^+, $n = [36, 58]$) (Lifshitz 2000; Chen et al. 2008; Zhen et al. 2014). These newly formed fullerene cations subsequently reacted with isoleucine molecules to form fullerene/amino acid cluster cations, during 5.8−9.88 s, in the ion trap, and then entered the mass spectrometer for their detection.

Figure 1 depicts the resulting mass spectrum of the trapped fullerene/isoleucine cluster cations, showing that a series of cationic clusters have been generated and also showing many more new peaks. Fullerene cations C_n^+ with $n = 46$ up to 60, and four observed groups of fullerene/isoleucine clusters are labeled: monoisoleucine adducts ($(Ile)C_n^+$, $n = [36, 60]$), di-isoleucine adducts ($(Ile)_2C_n^+$, $n = [40, 60]$), tri-isoleucine adducts ($(Ile)_3C_n^+$, $n = [40, 58]$), and tetra-isoleucine adducts ($(Ile)_4C_n^+$, $n = [40, 58]$).

Based on that, we suggest that fullerene/isoleucine cluster cations are formed through collision formation reaction between fullerene cations and neutral isoleucine molecules (Bohme 2016; Zhen et al. 2019a, 2019b). The corresponding formation pathways for fullerene/isoleucine clusters are summarized as below:

$$\begin{aligned} Ile + C_n^+ &\longrightarrow (Ile)C_n^+, \quad n = [36, 60] \\ Ile + (Ile)C_n^+ &\longrightarrow (Ile)_2C_n^+, \quad n = [40, 60] \\ Ile + (Ile)_2C_n^+ &\longrightarrow (Ile)_3C_n^+, \quad n = [40, 58] \\ Ile + (Ile)_3C_n^+ &\longrightarrow (Ile)_4C_n^+, \quad n = [40, 58]. \end{aligned}$$

Furthermore, we performed another experiment adopting the stored waveform inverse Fourier-transform excitation (SWIFT; Doroshenko & Cotter 1996) isolation technique, which clearly demonstrated the formation toward clusters of each individual fullerene cations. In that experiment, when the laser irradiation ended, a SWIFT pulse was applied to the ion trap, allowing for the selection of the desired fullerene cations and understanding their reactions with isoleucine. Figure 2 displays a typical mass spectrum for the clusters formed between individual fullerene cations (in here, C_{50}^+) and isoleucine, where fullerene cations C_{50}^+ and clusters $(Ile)_{1-5}C_{50}^+$ were observed and labeled, especially for the largest clusters $(Ile)_5C_{50}^+$ ($m/z = 1255$, 160 atoms).

The chemical reactivity of fullerene cations can be qualitatively described by a rough measurement of the rate constants for the reaction of $C_n^+ + Ile$ (Tielens 2005). Under our reaction conditions (at ~300 K and at a pressure of $\sim 6.0 \times 10^{-7}$ mbar), the reactant isoleucine molecules effuse continuously toward the center of the ion trap and are in larger abundance than the fullerene ions. Therefore, we could maintain isoleucine at a constant amount, and the bimolecular reaction could then be assumed to follow pseudo-first-order kinetics.

For the reaction of $C_n^+ + Ile$, the rate can be expressed as

$$\frac{d[C_n]}{dt} = -K[C_n]. \tag{1}$$

Integrating in terms of $d[C_n]$ and dt, we could obtain

$$\frac{[C_n]}{[C_n]_0} = \exp(-Kt); \quad K = k[Ile] + k_n, \tag{2}$$

where K is the pseudo-first-order rate constant for C_n^+ due to reaction loss, k is the bimolecular rate constant for the reaction of C_n^+ with isoleucine, k_n is the loss rate constant for fullerene ions due to reaction and diffusion in the absence of isoleucine. t is the reaction time, $[C_n]$ is the amount of fullerene cations at the moment of t, and $[C_n]_0$ is the initial amount of fullerene cations at the beginning of the reaction.

The ratio $[C_n]/[C_n]_0$ equals to I/I_0, where I and I_0 are the species intensities in the mass spectrum at the final and initial moments of the reaction, respectively. I_0 can be obtained using the intensity sum of the species that contained the special

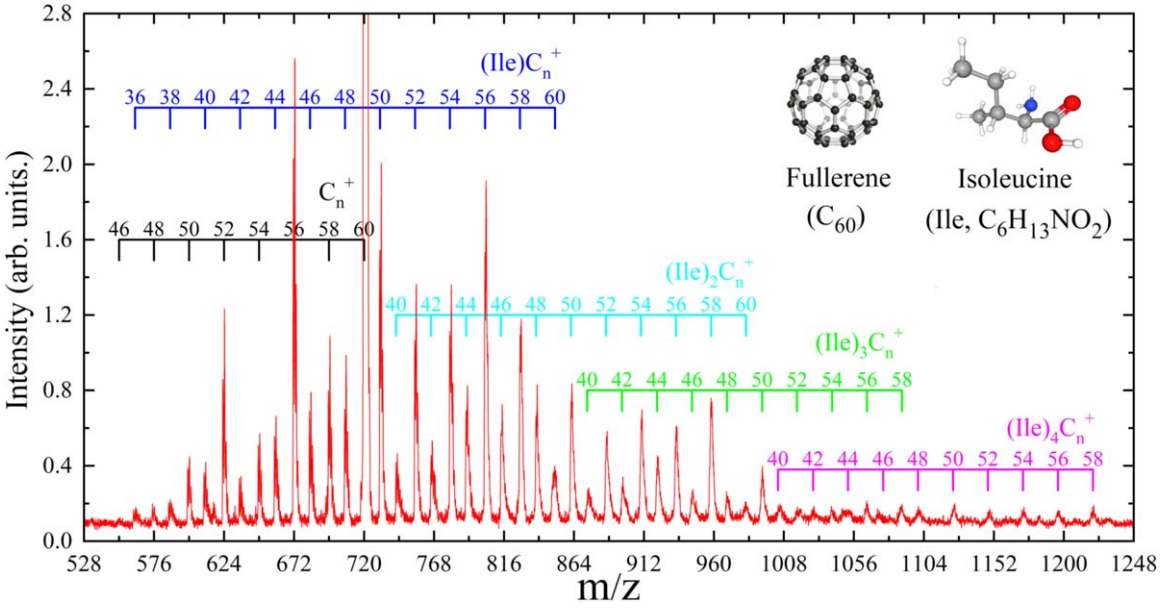

Figure 1. The resulting mass spectrum of trapped fullerene/isoleucine cluster cations. A 355 nm laser with the energy of 30 mJ/pulse and irradiation time amounting to 1.8 s (4.0−5.8 s). After irradiation, collision reactions between fullerene cations and isoleucine occurred in the period of 5.8−9.88 s.

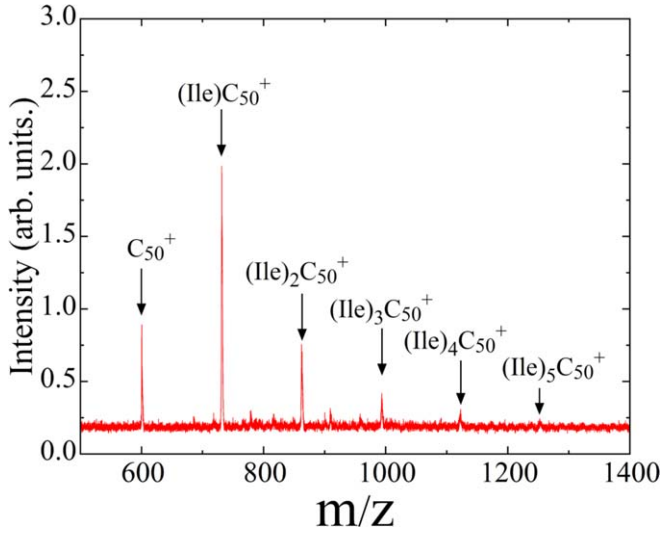

Figure 2. The resulting mass spectrum of C_{50}^+/isoleucine cluster cations with SWIFT technique. When the irradiation was finished at 5.8 s, SWIFT technique (5.8−6.0 s) was employed. Collision reaction between desired fullerene cations and isoleucine then occurred (6.0−9.88 s).

fullerene cations. For example, I_0 for C_{60}^+ can be measured as the intensity sum of C_{60}^+ and all C_{60}^+/isoleucine clusters at the initial moment of the reaction. Each species intensity is obtained from the mass spectrum by integrating the corresponding mass peaks.

To determine the rate constants, the mass spectra are recorded at different times ($t = 1.78$, 2.28, 2.78, 3.28, 4.08, and 4.88 s) are recorded under the same experimental conditions by adjusting the introduction time of the ions from the trap in each measurement. I_0 can be easily maintained as a constant during each reaction time, but it becomes difficult to be maintained as a constant during the time of multiple time measurement. Therefore, we cannot generate semilogarithmic plots to establish exponential behavior as is usually done to deduce the magnitude of the rate constant. Instead, a two-point kinetic analysis is used to roughly estimate the rate constants, one point taken at the beginning and one at the end of the reaction time.

Figure 3 shows the obtained values of I_0, I/I_0 and the roughly determined rate constants k for the reaction of C_n^+ with isoleucine at reaction time 4.08 s (5.8-9.88 s). Figure 3 (A) depicts the initial intensity I_0 of all detected fullerene cations. The global trend is that the initial intensities decrease gradually as the carbon atom number becomes small. The magic number of C-atom counts (60, 56, 50, and 44) that are more intense compared to neighboring peaks are observed in the present experiment, in agreement with previous works (Handschuh et al. 1995; Lifshitz 2000; Zhen et al. 2014).

Figure 3(B) depicts the final-to-initial intensity ratio (I/I_0) for all detected fullerene cations. There exists an obvious difference for the I/I_0 values among fullerene ions: the I/I_0 ratio for C_{60}^+ is nearly 1, but it is significantly lower for smaller fullerene cations. In the case of fullerene cations C_n^+, $n = [36, 44]$, their high chemical reactivity caused their prompt consumption during the reaction period (4.08 s), preventing us from pinning down the concentration ratio accurately. Hence, an upper limit is reported instead.

The pseudo-first-order rate constant K for each fullerene ion can be approximately measured by substituting the known I/I_0 and t (4.08 s) values into the rate equation. Based on the approximate equation $K = k$[Ile], which neglects the loss rate constant of fullerene ions due to the loss process in the absence of isoleucine, e.g., reaction, we determine the bimolecular rate constants for the reaction of fullerene ions and isoleucine, subsequently. By measuring the pressure difference in the ion trap chamber with and without adding isoleucine molecules, the concentration of isoleucine reactant, roughly a constant during the reaction, is estimated to be $\sim 1.0 \times 10^{10}$ molecule cm^{-3}. Figure 3(C) shows the bimolecular rate constants k for fullerene ions, where k for smaller fullerene ions are significantly larger than that for C_{60}^+. For fullerene cations (C_{58}^+ to C_{36}^+), k is larger than that for C_{60}^+ by one order of magnitude. Furthermore, the values of k for C_{58}^+ and C_{54}^+ manifest a remarkable enhancement, in comparison to its neighbor peaks.

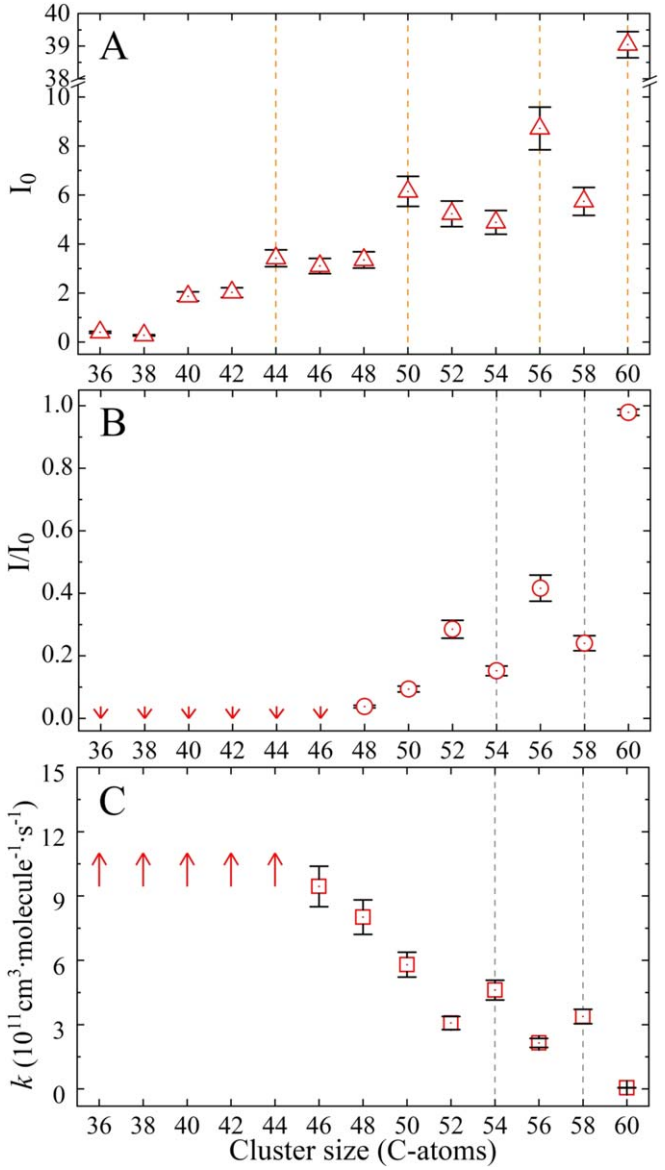

Figure 3. Panel (A): the initial intensity I_0 of all detected fullerene cations; Panel (B): the ratios (I/I_0) between final intensity and initial intensity for each fullerene cations; Panel (C): rate constants for the reaction of fullerene cations and isoleucine with the reaction time $t = 4.08$ s. The magic number of fullerenes and the reactivity magic number are indicated by orange and gray dot lines, respectively. The uncertainties given in the figures are one standard derivation.

Figure 4 displays the approximate values for bimolecular rate constants measured at different reaction time ($t = 1.78$, 2.28, 2.78, 3.28 and 4.08 s). Considering the uncertainty in reagent isoleucine concentration, i.e., the uncertainty in the pressure measurement, 10% uncertainty is given.

It can be seen that the rate constant k is minimally dependent on the reaction time, if its uncertainty is taken into account. Relatively short reaction times allow for measuring the rate constants for smaller fullerene ions C_n^+, $n = [36, 44]$, which turn out to be similar to that for C_{46}^+, given the large experimental error bars for the smaller fullerene ions. The approximate value of k for the reaction of fullerene ions with isoleucine are listed in Table 1. For fullerene cations, C_n^+, $n = [46, 60]$, the rate constants gradually increase as the fullerene's size decreases. The rate constants show similar

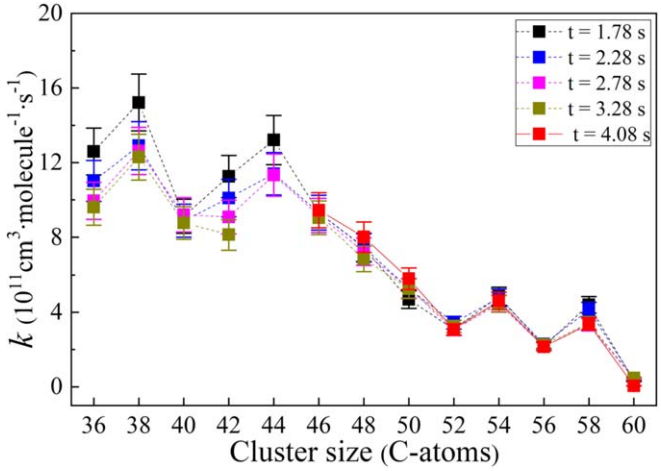

Figure 4. Rate constants for the reactions of C_n^+ + Ile with reaction time $t = 1.78$, 2.28, 2.78, 3.28, and 4.08 s. The uncertainties given in figures are one standard derivation.

Table 1
Rate Constants for the Reaction of Fullerene Ion with Isoleucine Molecules (in units of cm^3 molecule^{-1} s^{-1})

n	$k \times 10^{11}$	n	$k \times 10^{11}$
60	0.3 ± 0.03		
58	3.7 ± 0.4	46	9.3 ± 0.9
56	2.2 ± 0.2	44	7.2 ± 0.7
54	4.6 ± 0.5	42	7.7 ± 0.8
52	3.2 ± 0.3	40	7.2 ± 0.7
50	5.3 ± 0.5	38	10.6 ± 1.0
48	7.4 ± 0.7	36	8.6 ± 0.9

Note. The uncertainties are one standard derivation.

values when fullerene ions C_n^+ fall in the size range of $n = [36, 44]$. Moreover, the enhancement of the rate constants for C_{58}^+ and C_{54}^+ compared to neighboring peaks, i.e., chemical reactivity magic number of fullerene ions with C-atom counts (58, 54), are observed.

3. Theoretical Calculation Results

The molecular geometries and the binding energies for fullerene/isoleucine adducts were calculated using density functional theory employing the hybrid functional B3LYP (Becke 1992; Lee et al. 1988) in conjunction with the 6-31+G (d,p) basis set. The Gaussian 16 program (Frisch et al. 2016) packages were used for the calculations. To better describe the intermolecular van der Waals forces, the D3 version of Grimme's correction with Becke–Johnson damping is considered in the calculations (Grimme et al. 2011).

Since these species, including fullerene cations (C_n^+) and their monoisoleucine adducts (Ile)C_n^+, have an open-shell electronic structure, the doublet spin multiplicity is considered in the calculation. All the molecular geometries were optimized to the local minima of their potential energy surfaces. The basis set-superposition error correction (Basiuk & Tahuilan-Anguiano 2019) has a slight influence on binding energies and therefore was not included in current calculations. (Tables 2 and 3 list the calculated energies for all the species shown in Figures 5–7 is available in the supporting information).

The geometries of fullerene cations (C_n^+, $n = [52, 60]$) were first optimized and the structures are presented in Figure 5. We

Table 2
Calculated Energies for All the Species Listed in Figures 5–7 (unit: Hartree)

Species (Figure 5)	Energy	Species (Figure 6)	Energy	Species (Figure 7)	Energy
C_{60}^+	−2286.263326	$[(C_6H_{13}NO_2)C_{60}]^+(P_1)$	−2728.058118	$[(C_6H_{13}NO_2)C_{54}]^+(P_2\text{-}P_1)$	−2499.048335
C_{58}^+	−2209.926893	$[(C_6H_{13}NO_2)C_{60}]^+(P_2)$	−2728.046162	$[(C_6H_{13}NO_2)C_{54}]^+(P_2\text{-}P_2)$	−2499.030465
C_{56}^+	−2133.580299	$[(C_6H_{13}NO_2)C_{60}]^+(P_3)$	⋯	$[(C_6H_{13}NO_2)C_{54}]^+(P_2\text{-}P_3)$	−2498.996305
$C_{54}^+(P_1)$	−2057.236627	$[(C_6H_{13}NO_2)C_{60}]^+(P_4)$	−2727.998347	$[(C_6H_{13}NO_2)C_{54}]^+(P_2\text{-}P_4)$	−2499.022045
$C_{54}^+(P_2)$	−2057.239328	$[(C_6H_{13}NO_2)C_{60}]^+(P_5)$	−2728.014672	$[(C_6H_{13}NO_2)C_{54}]^+(P_2\text{-}P_5)$	−2499.022300
$C_{54}^+(P_3)$	−2057.136133	$[(C_6H_{13}NO_2)C_{58}]^+(P_1)$	−2651.742496	$[(C_6H_{13}NO_2)C_{54}]^+(P_3\text{-}P_1)$	−2498.964471
$C_{52}^+(P_1)$	−1980.931381	$[(C_6H_{13}NO_2)C_{58}]^+(P_2)$	−2651.711805	$[(C_6H_{13}NO_2)C_{54}]^+(P_3\text{-}P_2)$	−2498.990054
$C_{52}^+(P_2)$	−1980.904416	$[(C_6H_{13}NO_2)C_{58}]^+(P_3)$	−2651.692060	$[(C_6H_{13}NO_2)C_{54}]^+(P_3\text{-}P_3)$	−2498.913041
$C_{52}^+(P_3)$	−1980.767959	$[(C_6H_{13}NO_2)C_{58}]^+(P_4)$	−2651.678948	$[(C_6H_{13}NO_2)C_{54}]^+(P_3\text{-}P_4)$	−2498.969122
$C_{52}^+(P_4)$	−1980.710051	$[(C_6H_{13}NO_2)C_{58}]^+(P_5)$	−2651.695621	$[(C_6H_{13}NO_2)C_{54}]^+(P_3\text{-}P_5)$	−2498.974450
$C_{52}^+(P_5)$	−1980.924066	$[(C_6H_{13}NO_2)C_{56}]^+(P_1)$	−2575.391512	$[(C_6H_{13}NO_2)C_{52}]^+(P_2\text{-}P_1)$	⋯
		$[(C_6H_{13}NO_2)C_{56}]^+(P_2)$	−2575.360182	$[(C_6H_{13}NO_2)C_{52}]^+(P_2\text{-}P_2)$	−2422.733369
		$[(C_6H_{13}NO_2)C_{56}]^+(P_3)$	−2575.340855	$[(C_6H_{13}NO_2)C_{52}]^+(P_2\text{-}P_3)$	⋯
		$[(C_6H_{13}NO_2)C_{56}]^+(P_4)$	−2575.328384	$[(C_6H_{13}NO_2)C_{52}]^+(P_2\text{-}P_4)$	−2422.695190
		$[(C_6H_{13}NO_2)C_{56}]^+(P_5)$	−2575.344680	$[(C_6H_{13}NO_2)C_{52}]^+(P_2\text{-}P_5)$	−2422.697450
		$C_6H_{13}NO_2$	−441.756791	$C_6H_{13}NO_2$	−441.756791

assume there is no carbon skeleton rearrangement for fullerene cations formed both in the electron impact ionization, or the photodissociation processes. For the fullerene cations (C_{56}^+ and C_{58}^+), the same isomers are considered as were reported in the previous study (Lifshitz 2000; Lee & Han 2004; Candian et al. 2019; Zhen et al. 2019a) are applied. The isomer with one 7 C-ring was selected for the C_{58}^+ study, and the isomer with two 7 C-rings in opposite cage position was selected for the C_{56}^+ study. Based on the geometry of C_{56}^+, after losing one C_2 unit, we identify three isomers for C_{54}^+ (P_1 to P_3): namely three 7 C-rings (P_1) that contain four 7 C-rings (P_1), two 8 C-rings (P_2), 7 C-ring and 11 C-ring (P_3), two 9 C-rings (P_4), and two 7 C-rings & 8 C-ring (P_5) isomers, respectively. Our computation results indicate that smaller fullerenes $C_{54/52}^+$ may have various geometries, and some of them feature the larger C-rings.

In addition, the chemical reactivity of amino acids strongly depends on their structure and its changes during chemical or biological processes (Engel & Macko 1997; Snyder 1997). Since in our study, amino acid molecules are all isolated in the gas phase, so we mainly suppose amino acid molecules in their neutral form (H_2N-CH(R)-COOH), not in their zwitterionic form (^+H_3N-CH(R)-COO^-) (Engel & Macko 1997). Previously experimental studies have been obtained the gas-phase conformers of the isoleucine based on the rotational spectroscopy (Lesarri et al. 2005), and the matrix isolation Fourier-transform infrared (FTIR) spectroscopy (Stepanian et al. 2013). Moreover, we assume that amino acid molecules maintain their chiral character during the heating process here (370 K for isoleucine).

To elucidate the formation behavior of fullerene/isoleucine cluster cations, we present the optimized structures and the binding energies for (Ile)C_n^+, $n = [56, 60]$ in Figure 6, and $n = [52, 54]$ in Figure 7. We noted that, for the interaction of fullerene ions with isoleucine, various routes are possible. Here, five representative formation pathways are calculated. For isoleucine molecules, active amino groups and acidic carboxyl groups are considered toward the formation of fullerene/isoleucine clusters, specifically with N-atoms (from the amino unit) and O atoms (from carbonyl and hydroxyl unit). For smaller fullerene cations, 7 C-ring and larger C-rings are considered in the adduct formation reactions (Zhen et al. 2019a, 2019b).

Figure 6 displays the geometries and binding energies for (Ile)C_{60}^+. The newly formed (Ile)C_{60}^+ (P_1) is held together by dative bonding between the C_{60}^+ unit and the isoleucine unit through an van der Waals bond. Van der Waals bonding is about dispersion and very weak compared to any kinds of bonding that involve polarity. (Ile)C_{60}^+ (P_1) is held together because of dative bonding between the fullerene cations, a strong Lewis acid, and the amino-N, a Lewis base. The reaction is exothermic with 1.0 eV. In the group of (Ile)C_{60}^+ (P_2), (Ile)C_{60}^+ (P_2) is the product of addition of the amine N–H bond to a C = C bond, the C_{60}^+ and isoleucine connected by one C–N single bond, and C is from C_{60}^+ and N is from the amino unit of isoleucine, and one hydrogen atom directly migrates from the amino unit to the nearby carbon and forms a C–H bond. This reaction is exothermic with 0.7 eV. For the other three isomers of (Ile)C_{60}^+ (P_3, P_4, and P_5), the positive or small negative binding energies derived from the calculation results may indicate that they cannot be formed and may not exist.

Similar to (Ile)C_{60}^+, for (Ile)$C_{58/56}^+$, the geometries, and binding energies are also presented in Figure 6. The calculated binding energies indicate that the most possible geometries are P_1, which with a C–N single bond in which C-atom is from the 7 C-ring of $C_{58/56}^+$ and the N-atom is from the amino unit of isoleucine. The reaction is exothermic with 1.6 eV for (Ile)C_{58}^+ (P_1), and 1.5 eV for (Ile)C_{56}^+ (P_1). For the other isomers of (Ile)$C_{58/56}^+$, the positive or small negative binding energies may indicate that they cannot be formed and may not exist. Therefore, based on the calculation result presented in Figure 6, we may conclude that C_{58}^+ have a higher chemical reactivity compared to C_{56}^+ and C_{60}^+ when reacting with isoleucine.

In an attempt to explain the enhanced chemical reactivity of smaller fullerene, we also calculated partial geometries and binding energies for smaller fullerene adducts, e.g., (Ile)$C_{54/52}^+$, as shown in Figure 7. The reactions between smaller fullerene cations with isoleucine relatively easily occur, resulting in a very large number of reaction pathways and very complex newly formed molecular clusters.

For example, of the possible geometries and binding for (Ile)C_{52}^+, we only consider the 11 C-ring of C_{52}^+. In the group of (Ile)C_{52}^+ (P_2), the C_{52}^+ and isoleucine are connected by one C–N single bond, C from the 11 C-ring of C_{52}^+ and N from the amino unit of isoleucine, and one hydrogen atom directly migrates from the amino unit to the nearby carbon and forms a C–H

Table 3
Coordinates for All Species in XYZ Format

(1) C_{60}^{+}:	(16) $[(C_6H_{13}NO_2)C_{58}]^{+}(P_1)$:	(27) $[(C_6H_{13}NO_2)C_{54}]^{+}(P_2\text{-}P_2)$:
C 2.61938400-1.26712700-2.06487000	C 3.84575600 2.04854700-0.83247600	C 2.80516100 3.31999700-0.06296000
C 1.84794600-0.46438800-3.00090900	C 3.08197300 2.06962700-2.07470900	C 2.94901200 2.83812000-1.39742000
C 1.84590800 0.92214400-2.89444500	C 1.90888100 2.81033100-2.16004500	C 1.77412200 2.76106100-2.18899900
C 2.61516000 1.57471200-1.84657600	C 1.45554500 3.60882800-1.01774200	C 0.46745600 2.99539000-1.61223700
C 3.35104000 0.80720600-0.94331900	C 2.14790600 3.51853300 0.20763600	C 0.37818900 3.62456700-0.37013600

Note. This table is published in its entirety in the electronic edition of the *Astrophysical Journal*. A portion is shown here for guidance regarding its form and content.
(This table is available in its entirety in machine-readable form.)

bond, and this reaction is exothermic with 5.7 eV. In the group of $(Ile)C_{52}^{+}$ (P_4 or P_5), the C_{52}^{+} and isoleucine connected by one C-O single bond, one C from the 11 C-ring of C_{52}^{+} and O from the acid unit of isoleucine, and one hydrogen atom directly migrates from the acid unit to the nearby carbon and form a C–H bond, and this reaction is exothermic with 4.6 or 4.7 eV, respectively. These calculation results show that the hydrogen migration from isoleucine to fullerenes becomes more important as the C-rings become larger. These pathways will release more energies and make the corresponding adducts more stable, which may account for the fact that smaller fullerenes have higher reactivity.

Overall, the theoretical calculation results are consistent with the experimental results. We can conclude that ion–molecule reaction between fullerene cations and amino acids readily occur, resulting in a very large number of reaction pathways and very complex molecular clusters. Smaller fullerene cations (e.g., C_{48}^{+}) have higher reactivity than larger fullerene cations (e.g., $C_{56/58/60}^{+}$) when reacting with isoleucine. C_{58}^{+} have a higher chemical reactivity with isoleucine as compared to C_{56}^{+} and C_{60}^{+}. In addition, we note that we only calculated and presented the initial step of adduct reaction in the beginning of ion–molecule collision reaction process. With some intramolecular isomerization processes, the other functional group of the amino acid may also add to the surface of the fullerene, especially when adduct reaction occurs with smaller fullerenes, which contains the special cage structure (e.g., 11 C-rings). And maybe in the formation process, possible dynamical processes play an important role, further studies will be required to address this issue.

4. Results, Discussion, and Astronomical Implications

In summary, we have investigated the formation of large fullerene-amino acid derivatives in the gas phase both experimentally and theoretically. Laboratory studies have revealed that both bottom-up and top-down formation routes toward fullerene C_{60} also involve the formation of smaller fullerenes (Lifshitz 2000; Berné & Tielens 2012; Zhen et al. 2014; Cami et al. 2018). In this work, a series of fullerene cations C_n^{+}, $n = [36, 58]$ are generated by photofragmentation of C_{60}. We detected adducts formed between fullerene cations and up to four amino acids: monoisoleucine adducts ($(Ile)C_n^{+}$, $n = [36, 60]$), di-isoleucine adducts ($(Ile)_2C_n^{+}$, $n = [40, 60]$), tri-isoleucine adducts ($(Ile)_3C_n^{+}$, $n = [40, 58]$), and tetra-isoleucine adducts ($(Ile)_4C_n^{+}$, $n = [40, 58]$), which demonstrate the importance of ion–molecule reactions to the formation of large and complex fullerene-amino acid derivatives, especially for the largest clusters $(Ile)_5C_{50}^{+}$ ($m/z = 1255$, 160 atoms).

The rate constants for the reactions of fullerenes with isoleucine are roughly determined under the pseudo-first-order reaction condition. For fullerene cations, C_n^{+}, $n = [46, 60]$, the reactivity gradually increases as the fullerene's size reduces. The higher reactivity of fullerene species may indicate that amino acid molecules or other related prebiotic compounds can accrete on small carbon dust grains in the ISM (Tielens 2013; Marin et al. 2020). The size of these fullerene/amino acid derived clusters approach to that of very small grains. If we set aside the limitations of our experimental conditions, we can make a relatively reasonable guess that such molecular clusters can continue to grow in their current size (possibly adduct on the previous adducted amino acid for a third layer of clusters), i.e., in a favorable environment of interstellar space, it may be possible to eventually form molecular clusters with the order of micrometers through the ways mentioned above (Jäger et al. 2009; Berné et al. 2015). Interestingly, the later adducted amino acid might form an amide bond with the previous adducted amino acid on the surface of clusters. These two interstellar species may form clusters with multi-shell structural features, and then this structure can connect with multi-amino bearing PAHs to form clusters in large size (Rapacioli et al. 2006; Candian et al. 2018).

The molecular structure diversity for small fullerenes may be responsible for their significantly higher reactivity. The small fullerenes generated by UV laser photolysis show diversity in their geometries, being caged, semi-caged, or planar (Berné & Tielens 2012; Candian et al. 2019). The quantum chemical calculations suggest that relatively small fullerenes tend to be open cage. The open-caged isomer may accelerate the reaction with an amino acid molecule. When fullerene ions C_n^{+} fall in the size range of $n = [36, 44]$, similar chemical reactivity is observed. A possible reason is that similar geometries in these fullerene ions result in similar reactivity.

Moreover, the chemical reactivity for C_{58}^{+} and C_{54}^{+} compared to neighboring peaks, i.e., the magic number chemical reactivity of fullerene ions with C-atom counts (58, 54), are observed in the reaction of fullerene ions with isoleucine molecules. The laboratory results also show that C_{60}^{+}, C_{56}^{+}, and C_{52}^{+} possess lower chemical reactivity, possibly related to their higher structural stability. This chemical stability indicator presented here may be corrected with the observed abundance for various fullerenes in space (Bohme 2016; Zhen et al. 2019a). In combination with the studies of Cami et al. (2018) and Candian et al. (2019), these data hint at fullerene C_{56}, rather than C_{54} and C_{58} may be observed in the ISM where C_{60} emissions were detected (Bernard-Salas et al. 2012). The confirmation of these fullerene species needs further observation data, e.g., provided by the James Webb Space Telescope (Candian et al. 2018; Cordiner et al. 2019).

The gas-phase routes and the ice-surface routes are all the main mechanism for the inclusion of amino acids in meteorites

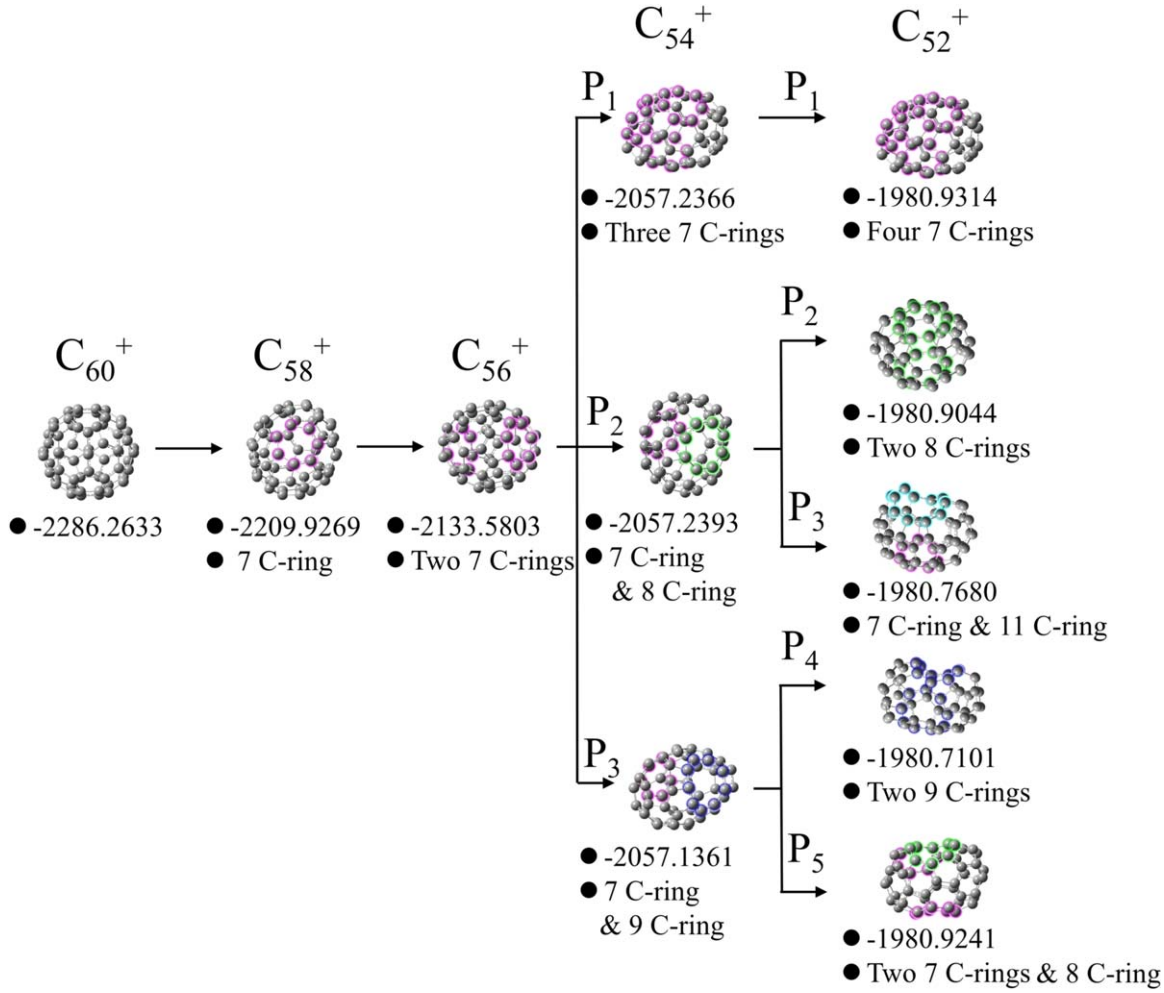

Figure 5. Optimized structures of fullerene ions C_n^+, $n = [52,60]$. Magenta carbon atoms for 7 C-ring, green carbon atoms for 8 C-ring, blue carbon atoms for 9 C-ring, and cyan carbon atoms for 11 C-ring. (units of energy: Hartree).

(Muńoz Caro et al. 2002; Jäger et al. 2009). Our present study indicates that small fullerene ions can form adducts with amino acid molecules much more readily than C_{60}^+. If these smaller fullerene ions are present in ISM, the formation of covalently bonding fullerene-amino acid derivate through ion–molecule reaction could provide a possible evolutionary path for the prebiotic amino acid molecules in the interstellar environments (together with the van der Waals clusters of C_{60}^+ with amino acid molecules). Amino acid molecules can accrete on small carbon dust grains through gas-phase routes, and then form larger carbon-bearing dust (Herbst & van Dishoeck 2009; Allamandola 2011).

5. Conclusions

In this work, the reactivity of fullerene cations is investigated by reaction with the astronomically relevant amino acid molecules (e.g., isoleucine) in the gas phase. A series of fullerene-amino acid cluster cations (e.g., $(Ile)C_n^+$, $n = [36, 60]$, $(Ile)_2C_n^+$, $n = [40, 60]$, $(Ile)_3C_n^+$, $n = [40, 58]$, $(Ile)_4C_n^+$, and $n = [40, 58]$) were formed with high efficiency through ion–molecule reactions. Rate constants for the cluster formation reactions between fullerene cations and mono-amino acid have been roughly estimated. Fullerene cations C_n^+, $n = [46, 60]$, show enhanced reactivity as the C-atom number decreases, while fullerene cations C_n^+, $n = [36, 44]$, show similar reactivity. Notably, the magic number chemical reactivity of fullerene ions with C-atom counts (58, 54) are observed. The experimental results provide a possible insight for searching the possible interstellar fullerenes (other than C_{60} and C_{70}) in terms of the chemical reactivity.

This work is supported by the Strategic Priority Research Program of Chinese Academy of Sciences, Grant No. XDB 41000000 and from the National Natural Science Foundation of China (NSFC, Grant No. 12073027, and Grant No. 41625013). Y.C. acknowledges the grant from the National Natural Science Foundation of China (NSFC, Grant No. 21827804). Theoretical calculations were performed on the Supercomputing Center of the University of Science and Technology of China.

Appendix
Experimental Methods

The experiment was performed in the setup equipped with the quadrupole ion trap and a reflection time-of-flight mass spectrometry. Briefly, fullerene molecule (C_{60}) was sublimated in an oven at a temperature of ~613 K and ionized by an electron gun (Jordan, C-950, ~82 eV). The fullerene cations of interest were then transported into the quadrupole ion trap

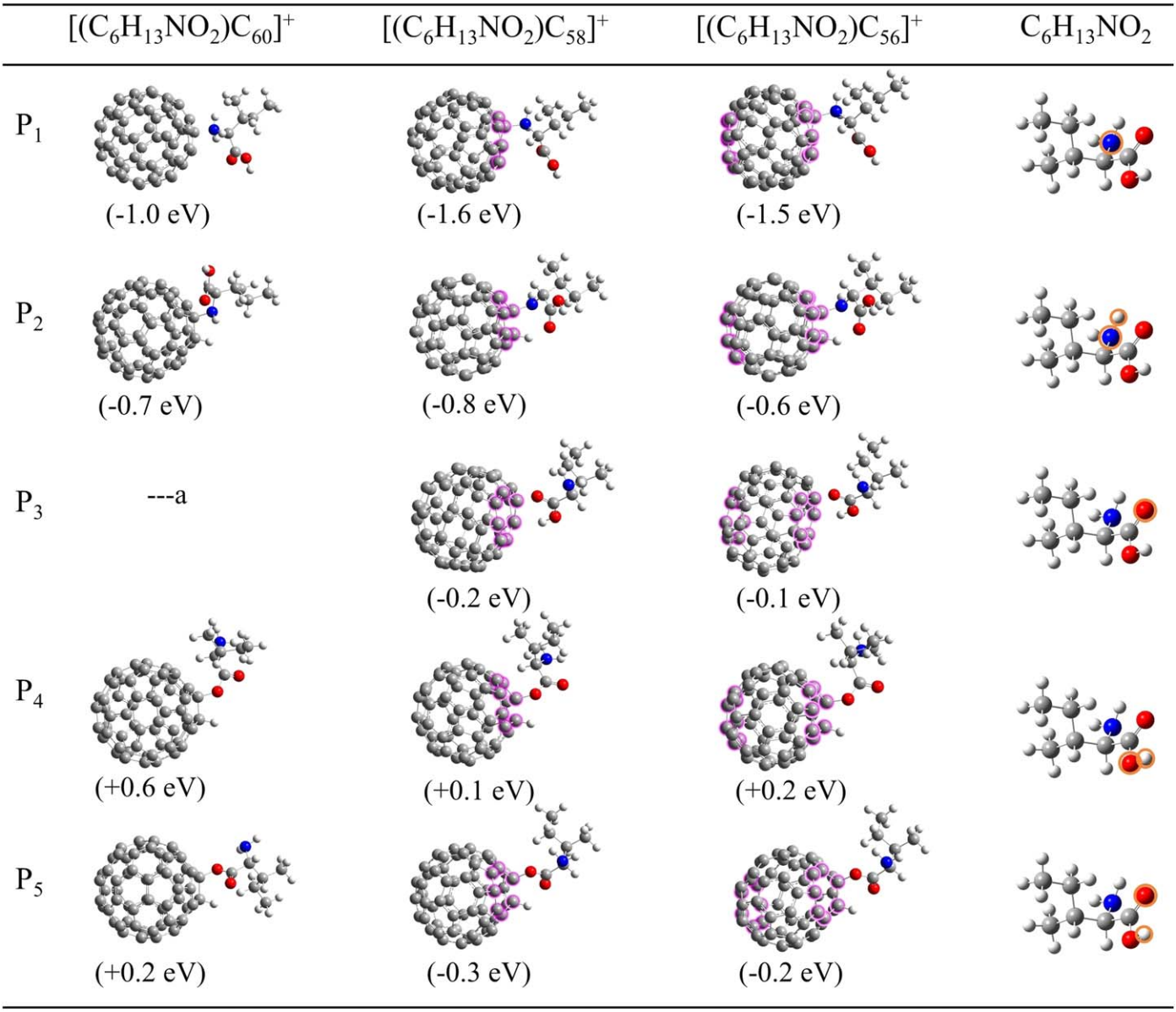

Figure 6. Optimized structures and binding energies for (Ile)C_{60}^+, (Ile)C_{58}^+ and (Ile)C_{56}^+. The feature marked with an "a" means that the dative bonding aggregate formed with the carbonyl-O turns into P_4 without a barrier.

(Jordan, C-1251) via an ion gate and a quadrupole mass filter (Ardara, Quad-925mm-01).

The gas-phase isoleucine molecules were produced by heating their powder (J&K Scientific, with purity better than 99%) in another oven (heating at ~380 K) mounted over the ion trap, which was effused continuously toward the center of the ion trap during the experiment. In the ion trap, fullerene/isoleucine cluster cations were formed through ion–molecule collision reactions between fullerene cations and isoleucine molecules. Buffer gas helium with high purity was used to thermalize the ions through collision (~300 K). The pressures in the ion trap chamber were $\sim 6.0 \times 10^{-7}$ and $\sim 2.0 \times 10^{-7}$ mbar in the cases with and without adding isoleucine molecules, respectively.

To generate a larger amount of photofragments small fullerene ions, a third harmonic output (355 nm) of a Nd:YAG laser (Spectra-Physics, INDI, pulse width ~6 ns, frequency 10 Hz) was used to irradiate the trapped fullerene cations and fullerene-amino acid cluster cations.

The whole set of experiments was conducted at a typically measured frequency of 0.1 Hz, i.e., each measurement period is 10 s. A high precision digital delay/pulse generator (SRS, DG535) was used to control the time sequence, which was set as follows:

(1) Without SWIFT isolation: The ion gate kept open during the time interval 0−4.0 s, allowing C_{60}^+ to accumulate to a certain amount, and the beam shutter then kept open during 4.0 −5.8 s, allowing trapped ions to be irradiated by a 355 nm laser beam. After the irradiation, the newly formed fullerene ions further reacted with isoleucine molecules for several seconds. At a proper moment, the ions were introduced out of the ion trap and then into a mass spectrometer for detection. In our experiment, these ions were introduced out of the trap at 6.58, 7.08, 7.58, 9.08, and 9.88 s in sequence, and the corresponding mass spectra were recorded;

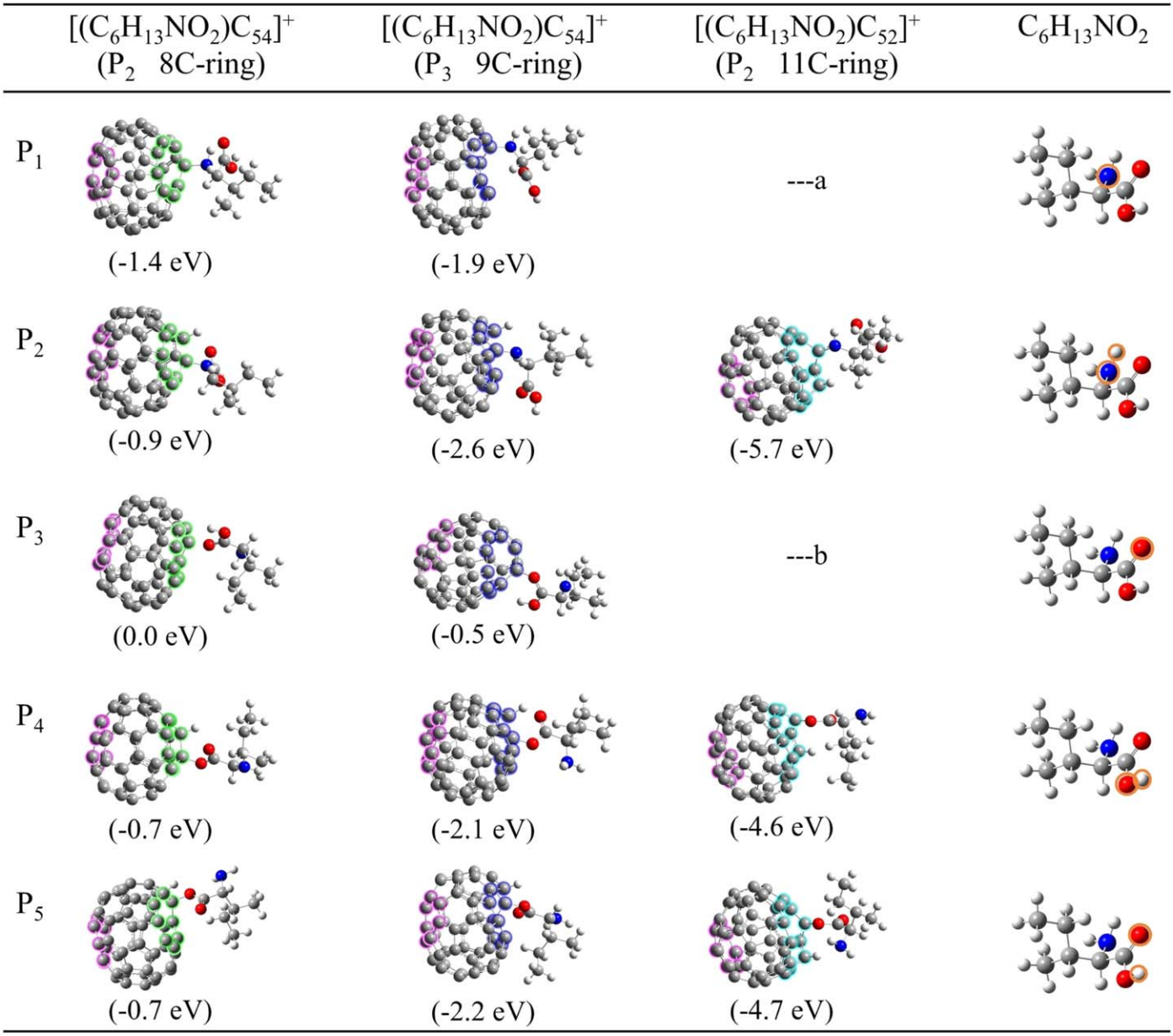

Figure 7. Optimized structures and binding energies for (Ile)C_{54}^{+} (8 C-ring), (Ile)C_{54}^{+} (9 C-ring), and (Ile)C_{52}^{+} (11 C-ring). The features marked with an "a" and "b" means that the dative bonding aggregates formed by C_{52}^{+} (11 C-ring) with the amino-N- or carbonyl-O atoms, respectively, turn into P_2 or P_4 without a barrier.

(2) With SWIFT isolation: The ion gate is kept open during the time interval 0−4.0 s, and the beam shutter is then kept open during 4.0−5.8 s. After the irradiation, a SWIFT isolation technique was employed to select the fullerene cations of interest (5.8−6.0 s). The selected ions then react with isoleucine molecules for 3.88 s (6.0−9.88 s). At 9.88 s, the ions were removed from the ion trap and then moved into a mass spectrometer to be detected.

References

Allamandola, L. J. 2011, EAS, 46, 305
Altwegg, K., Balsiger, H., Bar-Nun, A., et al. 2016, SciA, 2, e1600285
Basiuk, V. A., & Tahuilan-Anguiano, D. E. 2019, CPL, 722, 146
Becke, A. D. 1992, JChPh, 96, 2155
Bernard-Salas, J., Cami, J., Peeters, E., et al. 2012, ApJ, 757, 41
Berné, O., Montillaud, J., & Joblin, C. 2015, A&A, 577, A133
Berné, O., & Tielens, A. G. G. M. 2012, PNAS, 109, 401
Bohme, D. K. 2016, RSPTA, 374, 20150321
Briggs, J. B., & Miller, G. P. 2006, CRC, 9, 916
Cami, J., Bernard-Salas, J., Peeters, E., & Malek, S. E. 2010, Sci, 329, 1180
Cami, J., Peeters, E., Bernard-Salas, J., Doppmann, G., & De Buizer, J. 2018, Galax, 6, 101
Campbell, E. K., Holz, M., Gerlich, D., & Maier, J. P. 2015, Natur, 523, 322
Candian, A., Rachid, M. G., MacIsaac, H., Staroverov, V. N., Peeters, E., & Cami, J. 2019, MNRAS, 485, 1137
Candian, A., Zhen, J., & Tielens, A. G. G. M. 2018, PhT, 71, 38
Chen, De. T. W. Q., Feng, J., & Sun, C. 2008, JChPh, 128, 044318
Cordiner, M. A., Linnartz, H., Cox, N. L. J., et al. 2019, ApJL, 875, L28
Doroshenko, M. V., & Cotter, R. J. 1996, RCMS, 10, 65
Ehrenfreund, P., & Charnley, S. B. 2000, ARA&A, 38, 42
Engel, M. H., & Macko, S. A. 1997, Natur, 389, 265
Frisch, M. J., Trucks, G. W., Schlegel, H. B., et al. 2016, Gaussian, Inc 16, Revision e. 01 Wallingford, CT, Gaussian, Inc
García-Hernández, D. A., & Díaz-Luis, J. J. 2013a, A&A, 550, L6
Garcíia-Hernández, D. A., Cataldo, F., & Manchado, A. 2013b, MNRAS, 434, 415
Grimme, S., Ehrlich, S., & Goerigk, L. 2011, JCoCh, 32, 1456
Handschuh, H., Gantefor, G., Kessler, B., Bechthold, P. S., & Eberhardt, W. 1995, PRL, 74, 1095

Herbst, E., & van Dishoeck, E. F. 2009, ARA&A, 47, 427
Jäger, C., Huisken, F., Mutschke, H., Llamas Jansa, I., & Henning, T. 2009, ApJ, 696, 706
Jäger, C., Mutschke, H., Henning, T., & Huisken, F. 2011, EAS, 46, 293
Komatsu, K., Murata, Y., Wang, G. W., et al. 1999, FST, 7, 609
Kroto, H., Heath, J., O'Brien, S., Curl, R., & Smalley, R. 1985, Natur, 318, 162
Lee, C., Yang, W., & Parr, R. G. 1988, PhRvB, 37, 785
Lee, S. U., & Han, Y. 2004, JChPh, 121, 3941
Lesarri, A., Sanchez, R., Cocinero, E. J., Lopez, J. C., & Alonso, L. 2005, JACS, 127, 12952
Lifshitz, C. 2000, IJMS, 200, 423
Marin, L. G., Bejaoui, S., Haggmark, M., et al. 2020, ApJ, 889, 101
Muńoz Caro, G. M., Meierhenrich, U. J., Schutte, W. A., et al. 2002, Natur, 416, 403
Omont, A. 2016, A&A, 590, A52
Otero, G., Biddau, G., Sánchez-Sánchez, C., et al. 2008, Natur, 454, 865
Petrie, S., & Bohme, D. K. 1993, Natur, 365, 426
Pizzarello, S., Cooper, G. W., & Flynn, G. J. 2006, in Meteorites and the Early Solar System II, ed. D. Lauretta & H. McSween (Tucson: Arizona Press), 625, p
Rapacioli, M., Calvo, F., Joblin, C., et al. 2006, A&A, 460, 519
Sato, S., Maeda, Y., Guo, J., et al. 2013, JACS, 135, 5582
Snyder, L. E. 1997, Orig. Life Evol. Biosph., 27, 115
Stepanian, S. G., Yu, A., & Adamowicz, L. 2013, Chem. Phys., 423, 20
Tielens, A. G. G. M. 2005, The Physics and Chemistry of the Interstellar Medium (Cambridge: Cambridge Univ. Press)
Tielens, A. G. G. M. 2013, RvMP, 85, 1021
Zhen, J., Castellanos, P., Paardekooper, D. M., Linnartz, H., & Tielens, A. G. G. M. 2014, ApJL, 797, L30
Zhen, J., Zhang, W., Yang, Y., & Zhu, Q. 2019b, MNRAS, 490, 3498
Zhen, J., Zhang, W., Yang, Y., Zhu, Q., & Tielens, A. G. G. M. 2019a, ApJ, 887, 70
Zimmerman, J. A., Eyler, J. R., Bach, S. B. H., & McElvany, S. W. 1991, JChPh, 94, 3556